J. Fluid Mech. (1978), *vol.* 86, *part* 1, *pp.* 179–200
Printed in Great Britain

Kinematical studies of the flows around free or surface-mounted obstacles; applying topology to flow visualization

By J. C. R. HUNT,
Department of Applied Mathematics and Theoretical Physics, and Department of Engineering, University of Cambridge

C. J. ABELL,
Department of Engineering, University of Cambridge†

J. A. PETERKA AND H. WOO
Fluid Mechanics Program, Department of Civil Engineering, Colorado State University, Fort Collins

(Received 21 February 1977 and in revised form 9 August 1977)

In flows around three-dimensional surface obstacles in laminar or turbulent streams there are a number of points where the shear stress or where two or more components of the mean velocity are zero. In the first part of this paper we summarize and extend the kinematical theory for the flow near these points, particularly by emphasizing the topological classification of these points as nodes or saddles. We show that the zero-shear-stress points on the surface and on the obstacle must be such that the sum of the nodes Σ_N and the sum of the saddles Σ_S satisfy

$$\Sigma_N - \Sigma_S = 0.$$

If the obstacle has a hole through it, such as a passageway under a building,

$$\Sigma_N - \Sigma_S = -2.$$

If the surface is a junction between two pipes,

$$\Sigma_N - \Sigma_S = -1.$$

We also consider, in two-dimensional plane sections of the flow, the points where the components of the mean velocity parallel to the planes are zero, both in the flow and near surfaces cutting the sections. The latter points are half-nodes N' or half-saddles S'. We find that

$$(\Sigma_N + \tfrac{1}{2}\Sigma_{N'}) - (\Sigma_{S'} + \tfrac{1}{2}\Sigma_{S'}) = 1 - n,$$

where n is the connectivity of the section of the flow considered.

In the second part new flow-visualization studies of laminar and turbulent flows around cuboids and axisymmetric humps (i.e. model hills) are reported. A new method of obtaining a high resolution of the surface shear-stress lines was used. These studies show how enumerating the nodes and saddle points acts as a check on the inferred flow pattern.

† Present address: Department of Mechanical Engineering, University of South Australia, Adelaide.

Two specific conclusions drawn from these studies are that:

(i) for all the flows we observed, there are no closed surfaces of mean streamlines around the separated flows behind three-dimensional surface obstacles, which contradicts most of the previous suggestions for such flows (e.g. Halitsky 1968);

(ii) the separation streamline on the centre-line of a three-dimensional bluff obstacle does not, in general, reattach to the surface.

1. Introduction

There are still many simple flows where one does not know even the broad patterns of the streamlines, instantaneously or in the mean, let alone the magnitudes of the velocity and pressure. One such class of flows consists of moderate or high Reynolds number flows around (i) non-axisymmetric or non-cylindrical free-mounted bluff obstacles in uniform streams, (ii) any bluff obstacles in non-uniform streams and (iii) any bluff obstacles attached to a rigid surface. Another practically important and related class of flows consists of internal flows (lacking symmetry) such as those in pipe junctions, manifolds, expansions, etc.

The complete pattern of these kinds of flows can be obtained only by experiment or by direct computation of the Navier–Stokes equation. (Limited regions of the flow are, of course, often amenable to analytical methods.) But even then the flow patterns deduced from flow-visualization studies, measurements or computation are usually incomplete and approximate. Sometimes there is a large variation in the flow pattern inferred from similar data obtained by different investigators.

Some of the difficulty and ambiguity in inferring flow patterns from experiment and computation may be overcome by the application of kinematical principles and theorems, which are all based on the assumption that the velocity field is a continuous vector field and which do not involve any dynamical principles. More specifically, the application of kinematical principles can furnish answers to some of the basic kinematical questions that one asks about complicated flow patterns derived from experiments or computations.

($Q1$) Is the inferred flow pattern *kinematically* possible, i.e. is the flow pattern compatible with a continuous and finite mean or instantaneous velocity field?

($Q2$) Given information about one aspect of the flow, e.g. streamlines in one or two planes of the flow or shear-stress patterns on part of a surface bounding the flow, can other aspects of the flow pattern be inferred?

($Q3$) How can a complex flow pattern be described or characterized more succinctly than by many tabulations or graphs of velocities and streamlines?

($Q4$) What happens to the flow pattern if the topological character of the surfaces which bound the flow is changed (e.g. if a pipe meets another pipe or a building has a passageway underneath it)?

In the first part of this paper (§ 2) we derive some new results and review some of the previous results governing the kinematics of fluid flow. Many of the early developments in the kinematics of fluid flow were concentrated on surface shear-stress patterns with a particular emphasis on aeronautical problems (Lighthill 1963; Legendre 1965). More recently the kinematics of the *streamline* patterns have been developed by Smith (1972, 1975) and Perry & Fairlie (1974). Our work is an extension of these studies.

We particularly concentrate on the flow near points on the surfaces bounding the

flow where the shear stress is zero. If these points are classified by their topological characteristics as saddles or nodes, rather than by their usual fluid flow characteristics as separation or attachment points, we can show that there are topological constraints governing the number of nodes minus the number of saddles. As is well known, the kinematic analysis also helps to elucidate from experimental shear-stress patterns whether a zero-shear-stress point is a separation or an attachment point. We show how the streamline patterns in any plane can also be examined in terms of nodes and saddles, but in this case a new concept of half-nodes and half-saddles has to be introduced. These results for streamlines are derived by topological rather than by calculus arguments, but are similar to those previously derived by Smith (1972) for conical flows.

In the second part of this paper (§ 3) we describe various flow-visualization experiments which we have performed in wind tunnels and water flumes at Colorado State University and Cambridge. We have studied laminar and turbulent flow around surface obstacles, such as cuboids and axisymmetric humps (i.e. simple models of buildings or hills). A novel technique for visualizing the surface flow pattern has been developed especially for these highly turbulent recirculating flows.

By synthesizing our results with those of other flow-visualization experiments [notably those of Sutton (see Thwaites 1960), Norman (1975) and Furuya & Miyata (1972)] and velocity measurements near bluff obstacles (notably those of Castro & Robins 1977), we deduce and sketch the patterns of the mean-flow streamlines and surface-stress lines. We make particular use of the observed flow pattern near the points on the surface where the shear stress is zero, and thence draw some new conclusions about the location of separation and attachment surface shear-stress lines and flow streamlines. That in turn leads to an important conclusion that, on the basis of existing experimental data, in the flow around surface-mounted obstacles closed streamline surfaces do not exist. This contradicts the widely quoted assumption of Halitsky (1968) that they do exist.

These methods of applying kinematical principles to deduce complicated flow patterns from experiment and computation can be applied to many types of flow other than the bluff-body flows considered here.

2. Geometrical and topological properties of surface shear-stress lines and streamlines

2.1. *Observing and interpreting surface flow patterns*

If the surface of a body (for example a model building together with the floor of a wind tunnel) is coated with a layer of oil containing a powder in suspension, then after a period of time the flow moves the particles of the suspension into a persistent pattern. We define a vector field

$$P_s(x, y) = (P_{s1}, P_{s2}), \tag{2.1}$$

which is parallel to the *mean* direction of particle displacements, averaged over all particles which arrive at (x, y), where (x, y) is a point on a surface at which the curvature is not singular. Therefore if a particle is displaced by (dx, dy), then on the average

$$dx/P_{s1} = dy/P_{s2}. \tag{2.2}$$

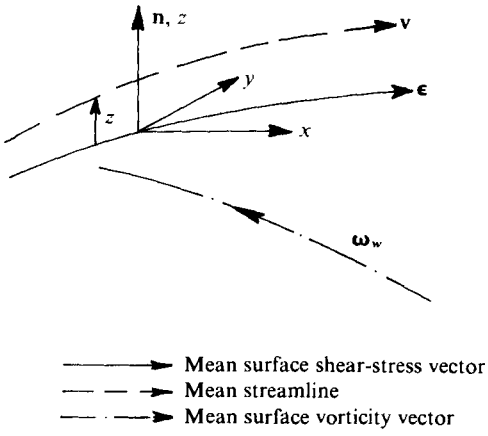

FIGURE 1. Sketch of the mean streamline immediately above and parallel to the mean surface shear-stress line.

Because of the damping effect of the oil, in a turbulent flow the particles in the suspension do not follow the random motions of air particles above the surface. But it is reasonable to assume that, provided the oil film is thin enough to be unaffected by pressure gradients (Squire 1962), the mean displacement of the particles in the suspension $\mathbf{P}_s$ is locally parallel to the mean velocity vector $\mathbf{v}$ of the air particles just above the surface. $\mathbf{v}(x, y)$ is defined as the average of the velocity of all fluid particles *arriving* at (x, y). This is not the same as the mean velocity of particles randomly released at (x, y), as is well known in the study of turbulent diffusion (e.g. Monin & Yaglom 1971, chap. 5).

Following Lighthill (1963), it is convenient to describe the mean velocity $\mathbf{v}(x, y)$ at a very small distance z from the surface in terms of the mean shear-stress vector $\boldsymbol{\epsilon}$ as

$$\mathbf{v} = (\boldsymbol{\epsilon}/\eta)\, z, \tag{2.3}$$

where

$$\mathbf{v} = (u, v), \quad \boldsymbol{\epsilon} = (\epsilon_u, \epsilon_v), \quad \boldsymbol{\epsilon} = \eta[\boldsymbol{\omega}_w \times \mathbf{n}], \tag{2.4}$$

$\boldsymbol{\omega}_w$ is the surface vorticity and $\mathbf{n}$ is the normal vector (see figure 1). By continuity, the vertical velocity component

$$w = -\tfrac{1}{2}\eta^{-1}\Delta z^2, \tag{2.5}$$

where

$$\Delta = \nabla . \boldsymbol{\epsilon} = \partial \epsilon_u/\partial x + \partial \epsilon_v/\partial y.$$

Whether or not $\mathbf{P}_s$ is exactly parallel to the mean velocity $\mathbf{v}$, $\mathbf{P}_s$ must be a continuous vector field with continuous derivatives, and be zero (i.e. $P_{s1} = P_{s2} = 0$) at only a finite number of points over the surface. Our strongest assumptions in analysing oil-film experiments are that where $\mathbf{P}_s = 0$, $\mathbf{v} = 0$ and that the characteristics of $\mathbf{P}_s$ and $\mathbf{v}$ (in the sense defined in § 2.2) near these points are the same.

2.2. *Classifying the singular points*

Singular points O on a surface are defined as those points where the shear stress is zero:

$$\epsilon_u = \epsilon_v = 0. \tag{2.6}$$

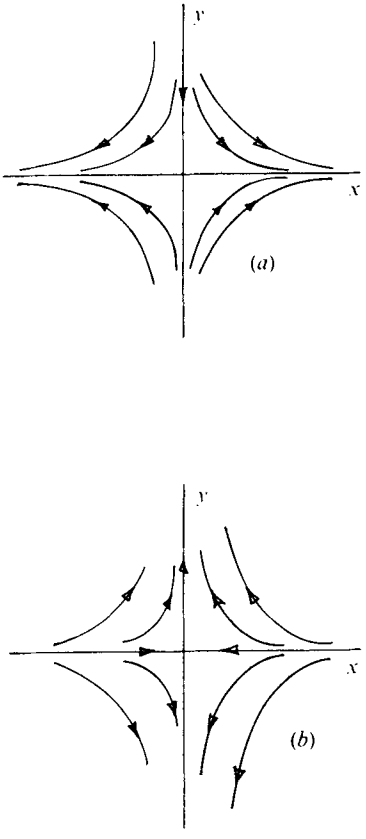

FIGURE 2. Saddle points ($J < 0$). (*a*) A separation point ($\Delta < 0$), where $\alpha < 1$ and $\partial\epsilon_v/\partial y > 0$. (*b*) An attachment point ($\Delta > 0$), where $\alpha > 1$ and $\partial\epsilon_v/\partial y < 0$.

Depending on the derivatives of ϵ_u and ϵ_v, in particular the divergence Δ and the Jacobian $J = \partial(\epsilon_u, \epsilon_v)/\partial(x, y)$, the singular points fall into two topological classes (see, for example, Lighthill 1963).

(i) *Saddle points* ($J < 0$) (figure 2), through which pass only two shear-stress lines (the critical lines), on each of which the direction of $\boldsymbol{\epsilon}$ changes sign, both directions being towards O on one and both away from O on the other.

(ii) *Nodal points* ($J > 0$), through which pass an infinite number of shear-stress lines, either all into the point or all out of the point. At a regular nodal point ($\frac{1}{4}\Delta^2 > J > 0$) two straight critical lines through O exist (figure 3). The other kind of nodal point is a *focus* ($J > \frac{1}{4}\Delta^2$), where all the shear-stress lines spiral into or out of O (figure 4).

This classification is quite different to that in terms of separation points (where $\Delta < 0$) and attachment points (where $\Delta > 0$).

By expanding $\boldsymbol{\epsilon}$ in terms of derivatives of its components one can also deduce the pattern of shear-stress lines near singular points. Consider the special case where (*a*) the critical lines are mutually perpendicular and (*b*) the streamlines are symmetric about the x, y axes, so that $\partial\epsilon_u/\partial y = \partial\epsilon_v/\partial x = 0$. At a *saddle point* the shear-stress lines are described by

$$y = Cx^{-\alpha}, \quad \text{where} \quad \alpha = |(\partial\epsilon_v/\partial y)/(\partial\epsilon_u/\partial x)| = [1 - \Delta/(\partial\epsilon_v/\partial y)]^{-1} \tag{2.7}$$

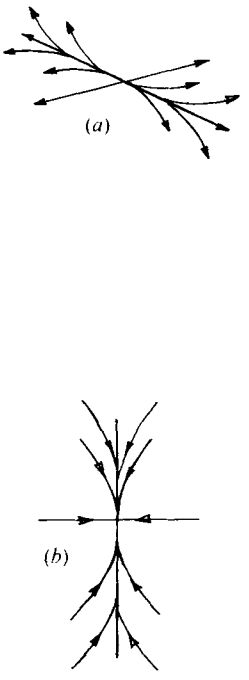

FIGURE 3. Nodal points which are not foci ($\frac{1}{4}\Delta^2 > J > 0$). (*a*) Attachment point, $\Delta > 0$. (*b*) Separation point, $\Delta < 0$.

and C is a constant along each line. Thus the shear-stress lines tend to converge more towards the x or y axis depending on whether

$$\alpha \gtrless 1 \quad (\text{or } \Delta/(\partial \epsilon_v/\partial y) \gtrless 0). \tag{2.8a}$$

Rarely, if ever, does $\Delta = 0$ or $\alpha = 1$ at a saddle point.

For a regular node ($\frac{1}{4}\Delta^2 \geqslant J > 0$), $y = Cx^{\alpha}$, where $\alpha = [\Delta/(\partial \epsilon_v/\partial y) - 1]^{-1}$. Note that $\Delta/(\partial \epsilon_v/\partial y) > 1$ if $J > 0$. Depending on whether

$$\alpha \gtrless 1 \quad (\text{or } \Delta/(\partial \epsilon_v/\partial y) \gtrless 2), \tag{2.8b}$$

shear-stress lines converge more towards the x or y axis (figure 3*b* or 3*a*).

From (2.8*a*, *b*) one can infer from observations whether a singular point is a separation or an attachment point. See § 3.

The critical shear-stress line at a saddle or node onto which all the shear-stress lines converge asymptotically is the line where the separated flow surface meets the plane $z = 0$. This is called a separation or attachment line depending on whether $\Delta \lessgtr 0$. Some distance from the zero-shear-stress point, a separation line can become an attachment line or vice versa without necessarily passing through another singular point.

Note that shear-stress lines, including the special cases of separation and attachment lines, may connect saddles to nodes, or nodes to nodes or saddles to saddles.

2.3. *Counting the number of zero-shear-stress points*

One of the main reasons for classifying the zero-shear-stress or singular points in topological terms as nodes and saddle points is because there is a relation between

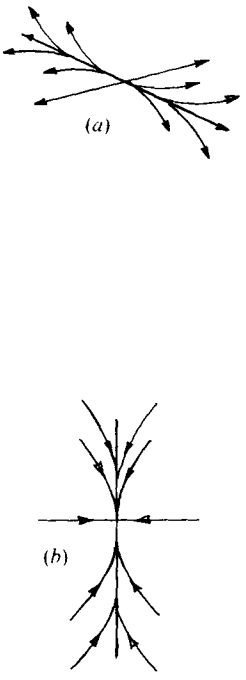

FIGURE 3. Nodal points which are not foci ($\frac{1}{4}\Delta^2 > J > 0$). (*a*) Attachment point, $\Delta > 0$. (*b*) Separation point, $\Delta < 0$.

and C is a constant along each line. Thus the shear-stress lines tend to converge more towards the x or y axis depending on whether

$$\alpha \gtrless 1 \quad (\text{or } \Delta/(\partial\epsilon_v/\partial y) \gtrless 0). \tag{2.8a}$$

Rarely, if ever, does $\Delta = 0$ or $\alpha = 1$ at a saddle point.

For a regular node ($\frac{1}{4}\Delta^2 \geqslant J > 0$), $y = Cx^\alpha$, where $\alpha = [\Delta/(\partial\epsilon_v/\partial y) - 1]^{-1}$. Note that $\Delta/(\partial\epsilon_v/\partial y) > 1$ if $J > 0$. Depending on whether

$$\alpha \gtrless 1 \quad (\text{or } \Delta/(\partial\epsilon_v/\partial y) \gtrless 2), \tag{2.8b}$$

shear-stress lines converge more towards the x or y axis (figure 3*b* or 3*a*).

From (2.8*a*, *b*) one can infer from observations whether a singular point is a separation or an attachment point. See § 3.

The critical shear-stress line at a saddle or node onto which all the shear-stress lines converge asymptotically is the line where the separated flow surface meets the plane $z = 0$. This is called a separation or attachment line depending on whether $\Delta \lessgtr 0$. Some distance from the zero-shear-stress point, a separation line can become an attachment line or vice versa without necessarily passing through another singular point.

Note that shear-stress lines, including the special cases of separation and attachment lines, may connect saddles to nodes, or nodes to nodes or saddles to saddles.

2.3. *Counting the number of zero-shear-stress points*

One of the main reasons for classifying the zero-shear-stress or singular points in topological terms as nodes and saddle points is because there is a relation between

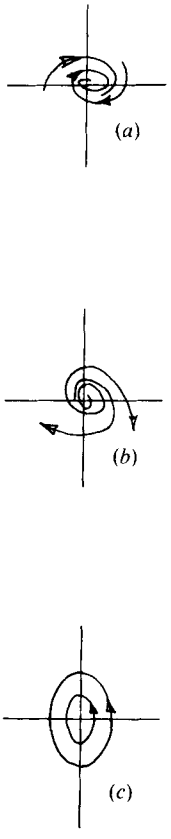

FIGURE 4. Nodal points which are foci ($J > \frac{1}{4}\Delta^2$). (*a*) Separation ($\Delta < 0$). (*b*) Attachment ($\Delta > 0$). (*c*) Neither separation nor attachment ($\Delta = 0$). (Not possible in a viscous flow at a finite Reynolds number.)

the number of nodes Σ_N and the number saddles Σ_S. For an isolated three-dimensional body, the topological equivalent of a sphere, there holds the well-known Poincaré–Bendixson (PB) theorem (more familiarly known as the 'hairy sphere' theorem) that

$$\Sigma_N - \Sigma_S = 2 \tag{2.9}$$

(Lighthill 1963; or Flegg 1974).

This result needs to be modified before being applied to the flow around a three-dimensional body B placed on a plane P. We can regard the plane as the upper surface of an imaginary three-dimensional body. The total number of nodes minus the total number of saddles, $\Sigma_N - \Sigma_S$, on the imaginary body must be the same whether B is on the plane or not. Therefore

$$(\Sigma_N - \Sigma_S)_{P+B} = 0. \tag{2.10}$$

In other words there must be two nodes, one upstream and one downstream at infinity; see figure 5. As we show in § 3, this result is useful for wind-tunnel investigations of three-dimensional obstacles.

It is also instructive to prove (2.10) by the PB theorem for the index of an isolated singular (or critical) point (Coddington & Levinson 1955, chap. 16). Assume that

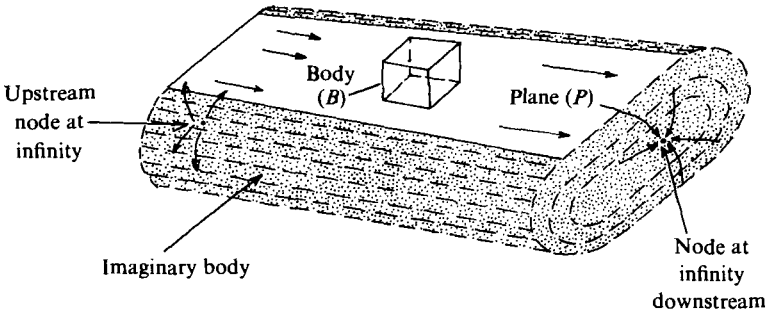

FIGURE 5. The imaginary three-dimensional body attached to the surface plane P and the real body B.

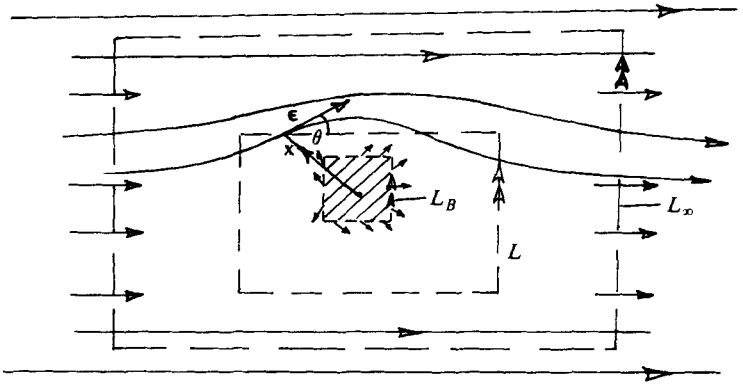

FIGURE 6. Showing how $\Delta\theta$ is calculated on the imaginary loops L, L_B and L_∞ drawn on the surface. – ⟶⟶, loops; ⟶⟶, typical shear-stress lines.

$\boldsymbol{\epsilon}(\mathbf{x}) = (\epsilon_u, \epsilon_v)$ is a continuous, bounded, real-valued vector function with only isolated singular points defined on a *plane* surface. θ is defined as the angle between $\boldsymbol{\epsilon}(\mathbf{x})$ and any fixed line, say the x axis (see figure 6). The PB theory shows that, if $\Delta\theta$ is the change in θ as $\mathbf{x}$ travels round a simple closed loop L on a plane, there being no singular points on L, then

$$\Delta\theta^{(L)}/2\pi = \Sigma_N^{(L)} - \Sigma_S^{(L)}, \tag{2.11}$$

where the superscript L on Σ denotes the number of singular points within L. Equation (2.11) is not necessarily true on a curved surface ($\Delta\theta^{(L)}$ is called the index in PB theory). If a loop L_∞ is taken far enough from the body on the plane where the shear-stress lines are parallel then, by inspection (see figure 6), $\Delta\theta^{(L_\infty)} = 0$, so (2.10) follows from (2.11). (If the surface on which the body lies is, say, part of a sphere (2.11) is not true. But if this part of the sphere were distorted onto a plane, then (2.11) could be applied and (2.10) would follow, because $\Sigma_N^{(L)} - \Sigma_S^{(L)}$ is not affected by topological distortions.)

Sometimes the nodes and saddles on the surface of the body are not known but the direction of the shear-stress lines is known on L_B, the line where the body meets the plane. Then by inspection of the shear-stress lines on L_B, $\Delta\theta^{(L_B)}$ and therefore $(\Sigma_N - \Sigma_S)_B$ on the body can be calculated. Thus in the example in figure 7

$$(\Sigma_N - \Sigma_S)_{B_1} = -1.$$

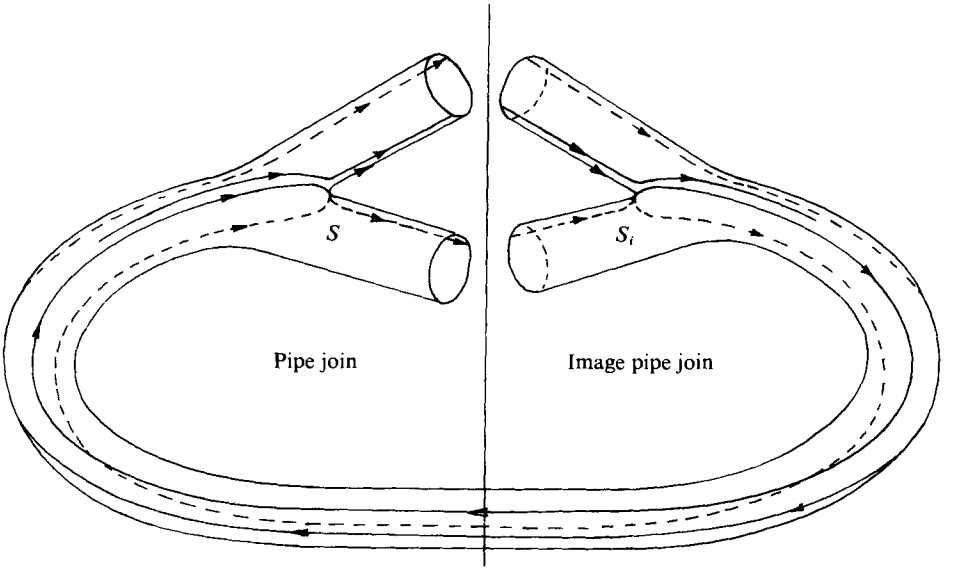

FIGURE 8. Zero-shear-stress points on the surface of two pipes where they join.

Now if the body has a hole through it (or a model building has a passageway underneath), as does the body B_2 in figure 7, then the surface plus the body become part of a *double* torus, for which the genus $g = 2$. Therefore

$$(\Sigma_N - \Sigma_S)_{P+B_2} = -2, \tag{2.13b}$$

i.e. there are two more saddle points than nodal points in such a flow.

Another problem is the junction of two pipes. First consider the surface shear-stress lines on the inner surface of the pipe; then consider an image pipe junction, as shown in figure 8, and finally connect the pipes together. A double torus results. Whence it follows that, if the subscript i denotes the singular points on the image pipe,

$$\Sigma_N + \Sigma_{N_i} - (\Sigma_S + \Sigma_{S_i}) = -2,$$

so that

$$\Sigma_N - \Sigma_S = -1. \tag{2.14}$$

In many pipe junctions it is observed that there are no nodes and one saddle point, as is shown to be topologically necessary by (2.19). An image system is often useful in the topological classification of flows.

2.5. *Mean streamline pattern*

If $\mathbf{v} = (u(x, y, z_0), v(x, y, z_0), w(x, y, z_0))$ is the mean velocity in the x, y plane for a constant value of z, say z_0, the plane may be bounded externally, say by a plane at $y = 0$, and internally by a body B. Then the mean streamlines are solutions of the equation

$$dx/u = dy/v. \tag{2.15}$$

Since $(u, v)(x, y)$ is a vector field $\mathbf{V}(x, y)$ with only a finite number of singular points in the interior of the flow at which $\mathbf{V} = 0$, it follows that saddle and nodal points can

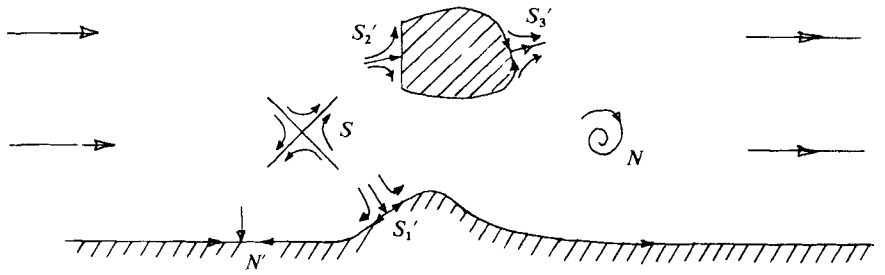

FIGURE 9. Saddle points and nodes in the streamline pattern on a section through the flow, denoted by S, N in the flow and S', N' on the surfaces. (The latter are half-saddles and half-nodes.)

be defined as in § 3. Perry & Fairlie (1974) made a special study of this particular application of the phase-plane theory of a differential equation. However, they did not attempt to develop an arithmetic for the number of nodes and saddle points.

Using calculus and contour-integration arguments for streamlines in *conical* flows, such as those around delta-wing aerofoils, Smith (1972) showed that there is a relation between the numbers of nodes and saddles for streamlines. A similar analysis can be used for any two-dimensional pattern of streamlines, in a two- or three-dimensional flow.† A more revealing argument (due mainly to Mr A. J. Casson of Trinity College, Cambridge) is exclusively topological.

Consider the streamlines in a two-dimensional plane $z = z_0$ which cuts a surface, and possibly one or more closed surfaces not connected to the surface in this plane (in which case the region is multiply connected). Let the nodes be labelled N and the saddles S. There will also be half-nodes or surface nodes N' and surface saddles S' (not to be confused with nodes and saddles in the shear-stress lines on the surface). See figure 9, in which only one body is located above the plane, so that the region is doubly connected.

First map the space above the surface into the region $OPXY$ shown in figure 10. The nature of each singular point is unchanged. Next consider an image space $O_i P_i X_i Y_i$ containing images of the nodes and saddles and an image body. Then connect the two spaces along OP and $O_i P_i$ and bend the surface into a cylinder until XY connects with $X_i Y_i$. Finally, stretch and indent the surfaces around B and B_i until B touches B_i, as shown in figure 11, and connect the ends of the cylinder to form a double torus. On the surface there are now only complete nodes and saddles; all the half-singular points S' and N' have been joined to their images, S_i' and N_i'.

Thus applying (2.12) and dividing by 2 leads to

$$(\Sigma_N + \tfrac{1}{2}\Sigma_{N'}) - (\Sigma_S + \tfrac{1}{2}\Sigma_{S'}) = 1 - n, \tag{2.16}$$

where this two-dimensional slice of the flow is n-tuply connected. For a singly connected region, with no body, $n = 1$; with one body present as in figure 9, $n = 2$; with

† In a three-dimensional flow these streamlines are not in general the projection of the three-dimensional streamlines onto the plane $z = z_0$, nor are they particle paths even in a steady flow. They are defined by (2.15).

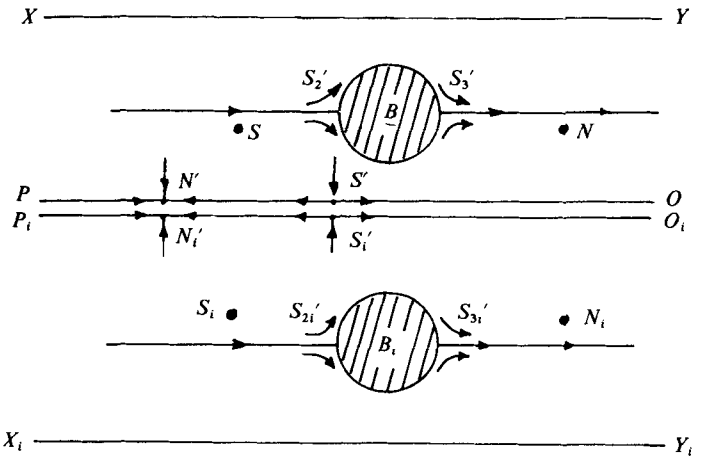

FIGURE 10. Mapping the flow in figure 9 onto $OPXY$ and the image system onto $O_i P_i X_i Y_i$.

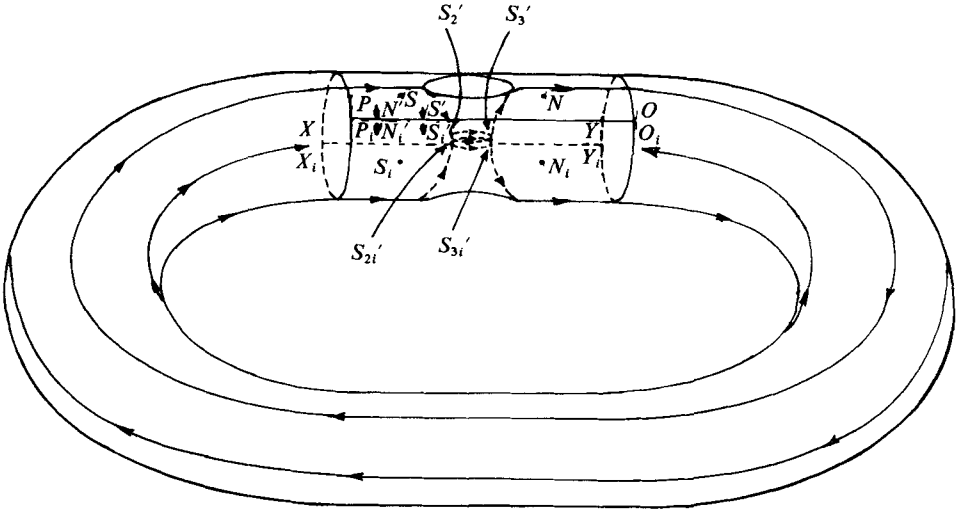

FIGURE 11. Mapping XYY_iX_i and the regions B, B_i onto the outside of a double torus.

two bodies present, $n = 3$. The result (2.16) is essentially the same as Smith's (1972) for conical flows.

A nice demonstration of this result (as was pointed out to us by M. J. Lighthill) can be given for potential flow past a circular cylinder when it has a circulation Γ around it (Batchelor 1976, p. 542). For Γ less than a critical value Γ_0, there are two surface stagnation points on the cylinder, so $-\frac{1}{2}\Sigma_{S'} = -1$, which agrees with (2.16) since $n = 2$. Then if for Γ greater than Γ_0 there are no singular points on the cylinder, the topological result (2.16) indicates that there must then be one saddle point in the flow since $-\Sigma_S = -1$, as indeed the dynamical calculations show.

Where the surface bounding the flow has a sharp angle, as for a cuboid on a plane, it has been proved by considering the locally low Reynolds number two-dimensional flow that there may be an *infinite* number of vortices with infinitely small velocity

squeezed into the corner (Moffatt 1964). Therefore in this case there will be, in principle, an infinite number of nodal points and saddle points in a finite area across the flow. Consequently there is, in general, no upper bound to Σ_N or Σ_S, and therefore more and more detail may be found by closer and closer inspection of flows with sharp bounding surfaces.

What are the consequences of observing only a finite number of these vortices? Provided that the 'truncated' streamline pattern is continuous, so that there are no unclosed streamlines pointing into or out of the corner, the neglected vortex pattern must contain an equal number of nodes and saddles [in the sense of (2.16)]. Consequently the observed or 'truncated' streamline pattern, which contains less detail and fewer nodes and saddle points than the actual flow, must satisfy (2.16). One might describe this as a 'kinematical truncation principle'.

3. Flow patterns from flow-visualization experiments

3.1. *Visualization techniques*

A novel oil-film technique was developed to obtain high resolution of mean shear-stress lines near singular points in highly turbulent flows. The film was a suspension of zinc oxide powder in 'Crisco' oil mixture. The mixture ratio (in volume) was 10% zinc oxide powder and 90% Crisco oil. The model was set on a Plexiglas base plate 0·96 m (38 in.) wide, 1·32 m (52 in.) long and 0·3 cm (0·125 in.) thick. The surface of the model and the base plate were coated uniformly with a layer of oil mixture. After the wind tunnel had been run for a period of time, the flow moved the suspended particles into a consistent pattern. A result such as those shown in figure 12 (plates 1 and 2) took about *one hour* to obtain.

The advantage of this method over the conventional use of titanium oxide in a light oil (Maltby & Keating 1962) for flows with low turbulence levels is that it avoids the excessive accumulation of powder at zero-shear-stress points. This can be particularly marked at foci (nodal singular points) downstream of surface obstacles. The disadvantage is the slowness of the development of the surface film.

Titanium tetrachloride was used for smoke studies at C.S.U. The smoke was either released from a bronze pipe, which could be held at any position in space, or injected inside the models and/or the base plate and then released from equally spaced holes on the surface of the model and base plate. The latter method gives significantly better resolution than the use of a single smoke source, especially for studying the flow pattern in the regions close to the base plate and model surfaces. Conventional paraffin oil smoke was used at Cambridge.

Flow-visualization experiments around bluff bodies can also be performed very effectively in water channels. Then dye released on the surface can indicate surface shear-stress patterns and the location of zero-shear-stress points, but not as well in a turbulent flow as good oil-film studies. In laminar flow streamlines can be more easily studied using dye and hydrogen bubbles in water than smoke in air. A masterly demonstration of this technique in the study of flows near surface obstacles has been given by Furuya & Miyata (1972). In rather less masterly fashion we did the same in slow-moving (< 5 cm/s) water flumes in Cambridge. Our experiments showed very clearly the connexion between surface shear-stress patterns and streamline patterns.

Such experiments give one confidence in inferring mean flow patterns from surface shear-stress patterns in complex turbulent flows.

3.2. *Surface flow pattern*

Using the oil-film visualization techniques described in § 3.1, the patterns of surface shear-stress lines have been observed in turbulent flows around cuboids with various shapes, placed at various angles to the flow, and in turbulent flows around axisymmetric humps. The experiments were performed in a large industrial aerodynamics wind tunnel (2×2 m) at Colorado State University (C.S.U.) and in small (e.g. 45×45 in.) wind tunnels at the University of Cambridge. At C.S.U. the boundary-layer thickness δ was 1·2 m and the heights h of the obstacles were about $\frac{1}{10}\delta$. (Further details are given by Woo, Peterka & Cermak 1976.) At Cambridge the ratio h/δ was about 5; the boundary layer and the free stream were turbulent. The intensity of the free turbulence was varied up to about 5%.

Figure 12 (plates 1 and 2) shows the oil-film flow patterns on the surface around (*a*) a cuboid ($h = 6{\cdot}5$ cm) perpendicular to the flow and (*b*) a cuboid at 47° to the flow. Here $h/\delta \simeq 0{\cdot}1$ and the Reynolds number for the cuboid $\simeq 7 \times 10^4$. It has often been noticed that the *patterns* are broadly similar whether $h/\delta \gg 1$ or $h/\delta \ll 1$ (e.g. Sharan 1975). The *positions* of zero-shear-stress points vary as h/δ varies and the number of such points upstream of the obstacle also varies. Similar patterns to those in figure 12 were found in our experiments at Cambridge when $h/\delta \simeq 5$ and $Re \simeq 4 \times 10^4$. In separate experiments the obstacles themselves were coated with an oil film, particularly to locate the positions of zero-stress points and separation and attachment lines. (For similar results see also Yu 1975.)

From these photographs and others, the surface shear-stress patterns over the surface and the obstacles were deduced. In drawing these patterns, sketched in figure 15, we have concentrated on the zero-shear-stress (or singular) points and the critical lines. Using the kinematical rules governing the shear-stress pattern on these lines, stated in § 2 and depicted in figures 2–4, we can identify which critical lines and singular points are separation and which are attachment lines and points. These are marked on the drawings. The exact nature of the flow near some critical points is difficult to discern from photographs. Sometimes only a study of the *movement* of the particles in the oil film enables a definite conclusion to be made.

In the shear-stress pattern on the plane around a cube (figure 13*b*), note that there are five saddle points ($(\Sigma_S)_P = 5$) and seven nodes ($(\Sigma_N)_P = 7$). Note that this figure is distorted to show all sides of the cube as well as the plane. By examining the *direction* of the shear-stress lines along L_B, the line where the cube meets the plane, we find that $\Delta\theta^{(L_B)} = -4\pi$. This agrees with the value of $\Delta\theta$ determined by the topological result (2.11) for this case where $(\Sigma_N - \Sigma_S)_P = -2$. It also means that on the cube there must be two more saddle points than nodes. For the cuboid at an angle to the flow (figure 13*c*), we have drawn only the surface shear-stress lines on the plane and ensured that (2.10) is satisfied.

The shear-stress pattern near the corners of the cube is not exactly clear. However we can tell whether there are more nodes than saddles or vice versa in any small region by calculating $\Delta\theta$ around a small circle surrounding the region. That is how we deduce that on only one of the corners, the rear upper corner, is there a node.

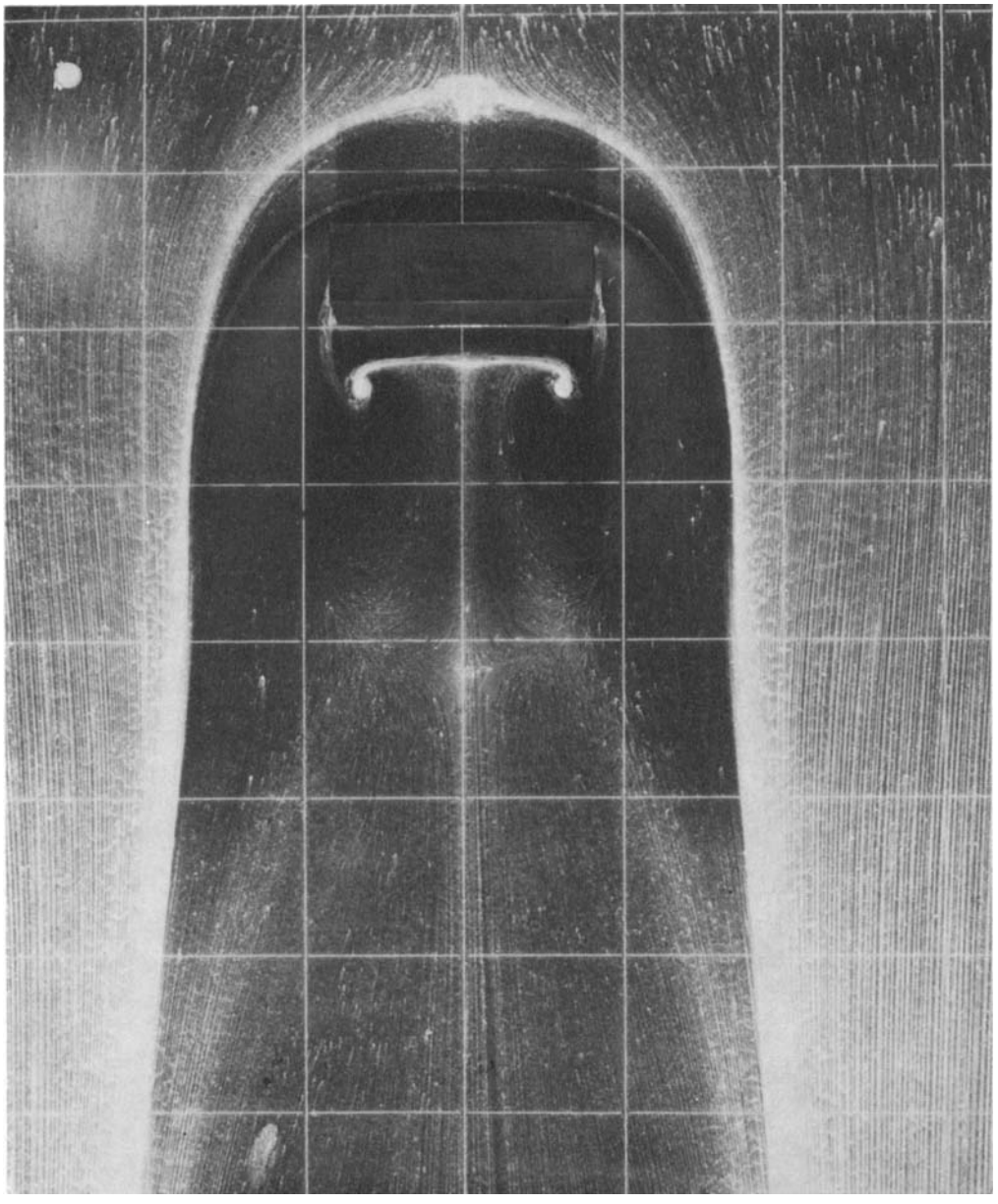

FIGURE 12 (*a*). For legend see plate 2.

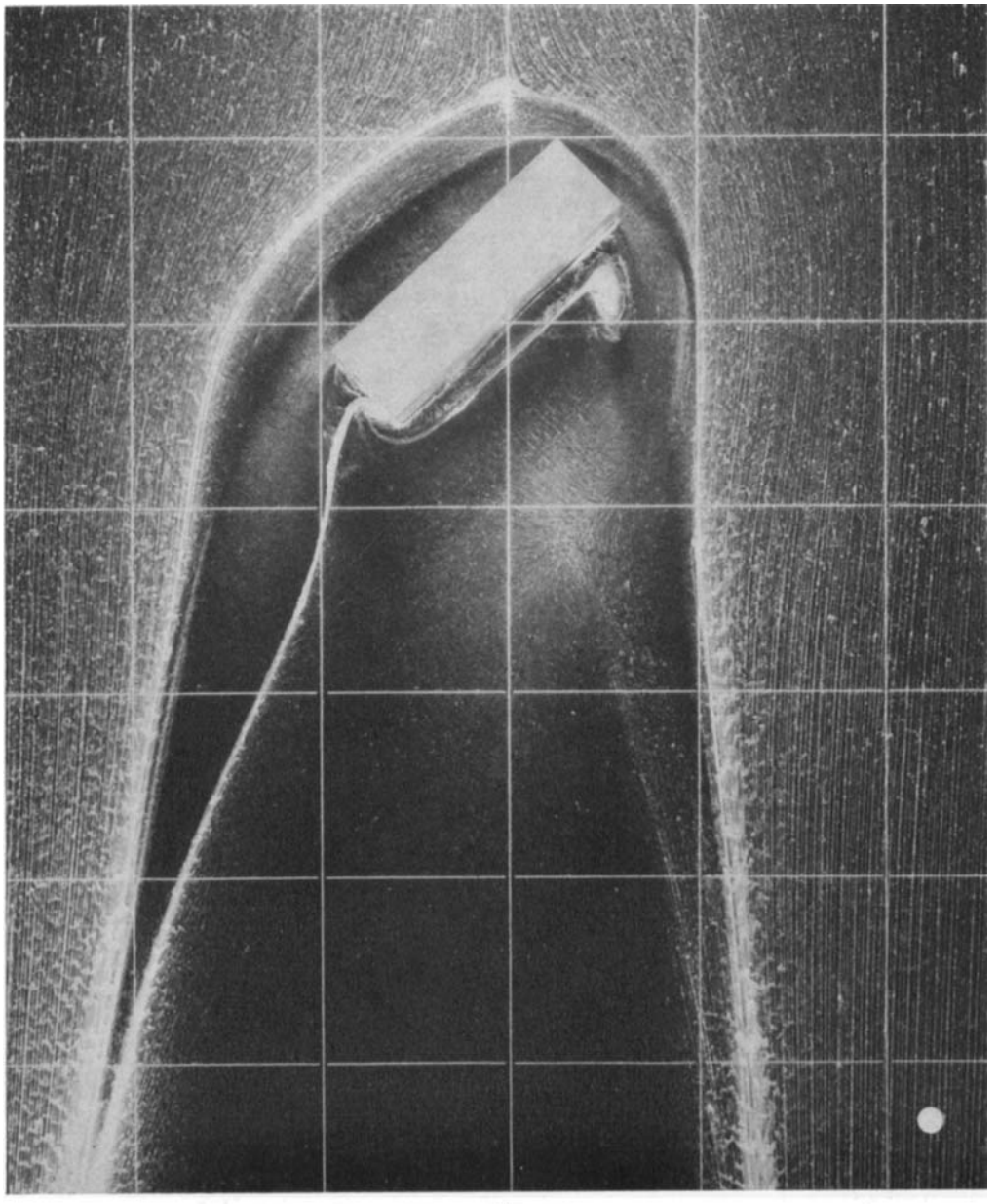

(*b*)

FIGURE 12. Photographs of the distribution of zinc oxide powder in Crisco oil on the surface of a wind tunnel around a cuboid ($6{\cdot}5 \times 6{\cdot}5 \times 20$ cm) (*a*) perpendicular to the flow and (*b*) at 47° to the flow.

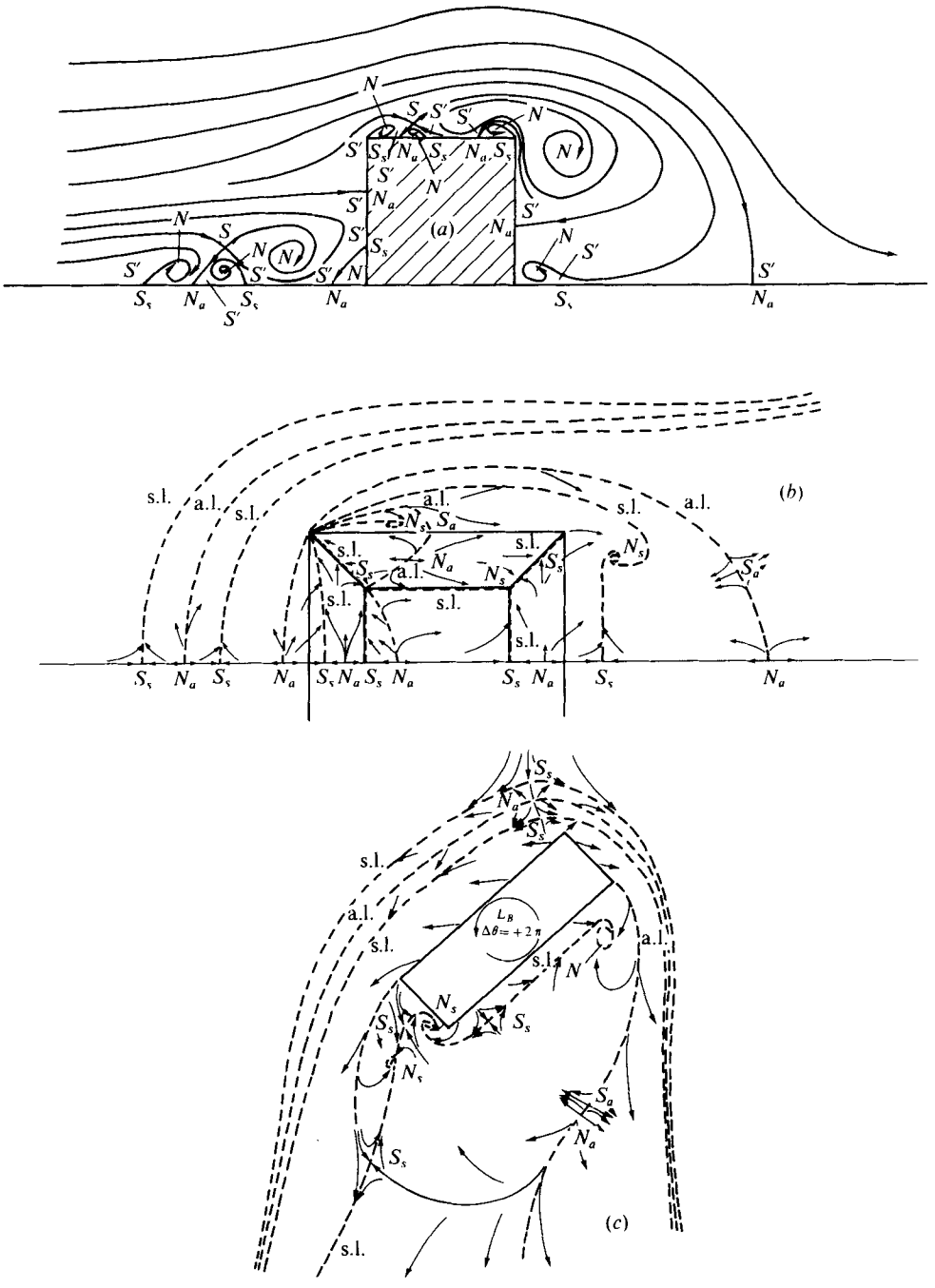

FIGURE 13. Shear-stress lines on the surface of a plane and on two cuboids, placed at different angles to the flow, based on our wind-tunnel experiments. (*a*) A cuboid (6·5 × 6·5 × 20 cm) perpendicular to the flow. (*b*) A cube (6·5 cm³) perpendicular to the flow. (*c*) A cuboid (6·5 × 6·5 × 20 cm) at 47° to the flow. ——→, shear-stress lines; – – –, shear-stress lines through singular points; s.l., separation lines; a.l., attachment lines; N, surface node; s, surface saddle; subscript s, separation; subscript a, attachment. (For clarity some fine detail has been excluded from (*a*). For further details see Woo *et al.* 1976.)

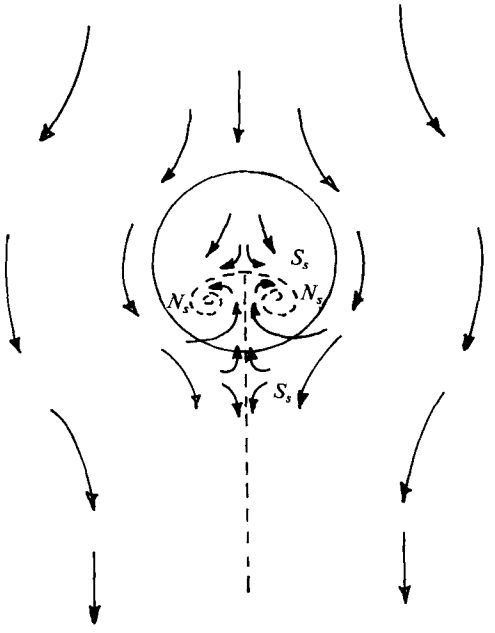

FIGURE 14. Shear-stress lines and zero-shear-stress points on the surface of an axisymmetric bell-shaped hump. Laminar flow; $Re \simeq 700$; maximum slope = 0·2.

Because of the difficulty of elucidating the shear-stress pattern near the corners, we also studied the surface and streamline flow pattern round axisymmetric bell-shaped hills; see figures 14 and 16. In laminar flow in a water channel at a low Reynolds number ($\simeq 700$) with $h/\delta \simeq \frac{1}{4}$, we observed the surface pattern shown in figure 14. The maximum slope of the hill is about 0·2. A somewhat different wake flow with a more complex flow structure was found at a higher Reynolds number ($\simeq 10^4$) in a turbulent boundary layer with $h/\delta \simeq 0{\cdot}1$ and a maximum hill slope of about 0·9. In that case a horseshoe vortex structure is observed upstream of the hill. Note particularly that in the laminar flow (figure 14) there is a *separation* line at right angles to the main flow direction passing through the downstream, nodal point. This critical line joins the upstream separation line at the upstream saddle point. But the most remarkable feature of the flow pattern in figure 14 is that *all* the singular, zero-shear-stress points are *separation* points. This flow is almost the simplest kind of three-dimensional separated flow and yet has this remarkable property. We found that at a Reynolds number of 700 a *cube* also has a separation line instead of an attachment line at the rear of the recirculating region in the wake.

3.3. *Mean streamline pattern*

From the surface flow patterns and information derived from visualization of the flow, by smoke, hydrogen bubbles, dye etc., we can sketch with some confidence the general pattern of the streamlines. On the basis of the similarity of the patterns of the surface shear-stress lines for different levels of turbulence and velocity profiles (or h/δ), it seems reasonable to use flow-visualization data from different flows to help draw conclusions as to the flow pattern.

In figures 15(*a*) and (*b*) the mean flow patterns round a cube and a cuboid in a turbulent boundary layer are sketched. The singular points in the flow and on the surfaces of the mean streamline patterns satisfy the topological constraint (2.16). For example, in figure 15(*b*)

$$\Sigma_N = 7, \quad \Sigma_S = 1, \quad \Sigma_{N'} = 0, \quad \Sigma_{S'} = 12,$$

so that

$$(\Sigma_N + \tfrac{1}{2}\Sigma_{N'}) - (\Sigma_S + \tfrac{1}{2}\Sigma_{S'}) = 7 - (1+6) = 0.$$

This agrees with (2.16), since the region is singly connected, so that $n = 1$. The mean streamlines, in a plane parallel to the upstream flow, off the centre-line are difficult to deduce and not very helpful for interpreting the flow. The overall flow pattern is best depicted by a three-dimensional sketch of the streamlines, such as that shown in figure 15(*c*).

Note that the separated flow over the upper surface of the cuboid does not reattach (figure 15*a*), which is a similar observation to others who have studied flow over two-dimensional surface prisms (e.g. Counihan, Hunt & Jackson 1974). On the other hand the separated flow over the cube does reattach (figure 15*b*), which is a similar finding to that of Castro & Robins (1977).

The streamlines in the horseshoe vortex pattern upstream of the obstacle are inferred from the mean surface shear-stress pattern and smoke visualization studies in laminar boundary layers by E. P. Sutton (see Thwaites 1960) and Norman (1975). Similar streamlines were previously deduced from Sutton's photographs by Perry & Fairlie (1974). It now seems to be a common observation that the number of vortices upstream is a sensitive function of the flow parameters. Up to seven vortices have been observed in some cases!

A particularly important practical question is whether there is, or is not, a closed mean streamline surface (otherwise knows as a 'bubble' or a 'cavity') in the wake of a surface-mounted bluff obstacle. The streamlines in figure 15 all show that this does not exist. Our reasoning is as follows. If such a surface exists, then it must pass through the centre-line separation point C_s (on the front or the rear of the top of the cuboid depending on whether the flow does not or does reattach to the top) and through the zero-shear-stress point C_d at the downstream end of the recirculating flow region. There must then be a critical surface shear-stress line from C_s to C_d, and such a line would begin as a separation line and end as an attachment line. In fact we observe that there is no critical line from C_s to C_d in figure 15(*a*), (*b*) or (*c*); so for these cuboids we conclude that there is no closed surface in the wake. This conclusion must also follow from the detailed velocity measurements (using a pulsed-wire anemometer) around a cube at high Reynolds number in a turbulent flow by Castro & Robins (1977). They find that a trailing vortex pattern starts at the upper corners of the cube. Such a vortex can exist only if mean streamlines are drawn into it. It is kinematically inconsistent with a closed surface surrounding the obstacle.

A separate, but related, question is whether the mean streamline from the separation point C_s reattaches to the surface at C_d. There is no *kinematic* argument why this should not be so. A plausible *dynamical* explanation of the observed flow pattern over a cuboid at high Reynolds number is that it is due to the rolling-up of the vortex sheet from the top of the cuboid, and, if so, then streamlines enter the vortex both on and off the centre-line. In that case C_s cannot be connected to C_d by a mean streamline. In the limit in which the aspect ratio of the cuboid (i.e. the width normal to the

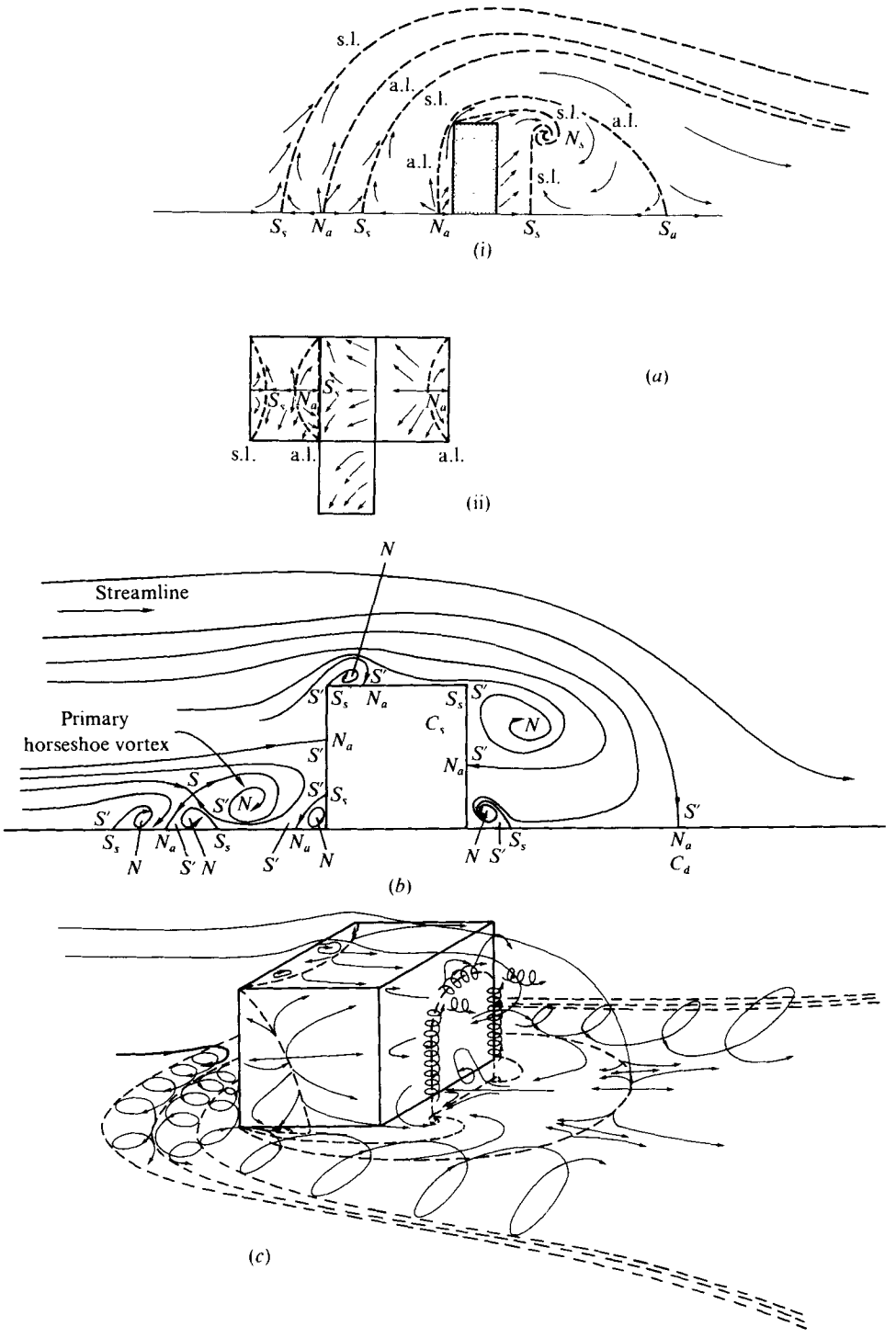

FIGURE 15. Mean streamlines, singular points and flow pattern around a cuboid and a cube. (*a*) On the centre-line of a cuboid. (i) Plan view of shear-stress lines on the surface. (ii) Shear-stress lines on the top and sides of the cube. (*b*) On the centre-line of a cube. (*c*) Sketch of the flow pattern around the cube. N, node of streamline pattern; S, S', saddles of streamline pattern; subscript s, separation; subscript a, attachment; N, surface node; S, surface saddle; C_s, centre-line separation point at rear of obstacle; C_d, downstream centre-line zero-stress point.

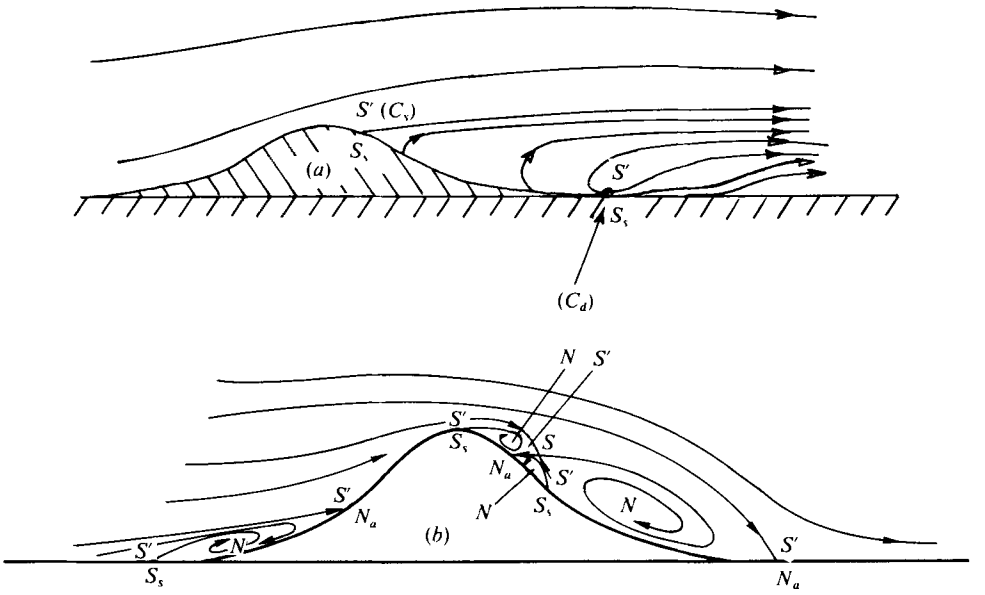

FIGURE 16. Mean streamlines and singular points on the centre-line plane of the flow over axisymmetric humps. (*a*) Laminar flow. (*b*) Turbulent flow.

flow/height) increases to infinity the streamline through C_s must approach that through C_d. From visualization of the flow behind a step in two and three dimensions Werlé (1975, see particularly his figure 4) draws similar conclusions.

The study of flow over a three-dimensional hump illuminates these questions. Figure 16 shows the centre-line streamlines over such humps in laminar flow and in turbulent flow. Clearly the flow over rounded obstacles, as with cylinders in two-dimensional flow, is more sensitive to the nature of the oncoming flow than the flow over obstacles with sharp edges. Figure 16 (*a*) shows how in a laminar flow, when there are only separation points on the surface, there can be no closed surface of mean streamlines and no streamline connecting C_s to C_d. The wake flow pattern we observed is very similar to those observed by Furuya & Miyata (1972) and Mochizuki (1961) over spheres on a plane in laminar boundary layers. None of these authors drew mean streamlines but from their dye and smoke photographs their flows in the wake would seem to be described by their sketch of the streamlines. Furuya & Miyata's and Mochizuki's observations show that, as their Reynolds number was increased and vortex shedding began, the mean streamline from C_s began to approach the surface. This is the explanation for the different streamline pattern, sketched in figure 16 (*b*), which is deduced from smoke-visualization and water-flume observations at high Reynolds number ($\simeq 10^4$). Note that in the laminar flow (figure 16 *a*) no shear-generated horseshoe vortices were set up, mainly because of the very low slope of the hump. In laminar flow experiments on bluffer obstacles these horseshoe vortices are found to occur and probably affect the wake. (See Furuya & Miyata 1972; and also Gregory & Walker 1955.)

An interesting conclusion from these investigations of the flow around cuboids and humps is that there must be at least one value Re_{crit} of the Reynolds number for any

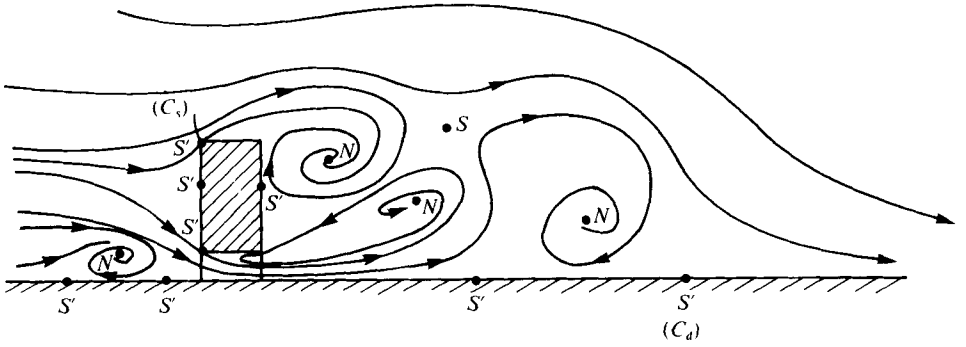

FIGURE 17. Mean streamlines and singular points observed in air flow around a cuboid (a model building) with a passageway underneath (same notation as figures 9 and 15).

given flow at which the mean streamline from P_s does reattach at P_d. For $Re < Re_{\text{crit}}$, the streamline does not reattach at all and for $Re > Re_{\text{crit}}$ the streamline rolls up. So at $Re = Re_{\text{crit}}$, it must reattach on the surface.

In figure 17 we have sketched the mean streamlines around a rectangular block which has a passageway underneath it. Many buildings have such shapes and it is important to know the flow patterns around them. The mean streamlines, which are sketched on the centre-line of the block, are based on smoke visualization and mean velocity measurements ($h/\delta \simeq 3$, $Re \simeq 4 \times 10^4$). The flow region on the centre-line is a doubly connected region ($n = 2$). We find that

$$\Sigma_N = 4, \quad \Sigma_{N'} = 0, \quad \Sigma_S = 1, \quad \Sigma_{S'} = 4,$$

so that

$$(\Sigma_N + \tfrac{1}{2}\Sigma_{N'}) - (\Sigma_S + \tfrac{1}{2}\Sigma_{S'}) = -1 = 1 - n,$$

in agreement with (2.16).

4. Conclusion

The main conclusion of this paper is that useful kinematical principles and theorems exist, some of which we have developed. These help the study of complicated flow patterns which are inferred from experiments or computations.

In the introduction we posed four basic questions that might be asked about a flow pattern. On the basis of §§ 2 and 3 here are some answers.

(1) If the topological constraints for the singular points of the surface shear stresses [equations (2.10) and (2.11)] and the streamlines [equation (2.16)] are not satisfied then the flows are kinematically impossible. Papers are not infrequently published containing such kinematically impossible flows.

(2) In complicated flows some useful information can be gained about one part of the flow from knowledge of the flow in another part, for example by finding $\Sigma_N - \Sigma_S$ on part of a surface over which the flow is unknown, or inferring from the shear-stress patterns at a singular point whether it is a separation or attachment point.

(3) We have discussed the flow around various three-dimensional surface obstacles in terms of the singular points of the shear stress and mean streamline pattern and in terms of the critical lines which emanate from these points. We have seen how the

character, location and number of these points and lines vary with the shape of the bluff body, the Reynolds number and the upstream flow conditions. This type of discussion enables one to pick out the salient similarities and differences among complex three-dimensional flows. Once the topological and attachment/separation character of these points and lines have been determined by visualization or computation, the general flow pattern is effectively determined. This is simpler and more economical than describing the flow solely in terms of a large number of diagrams of mean streamline patterns. Of course a few such diagrams are essential to an understanding of the flow.

(4) We have seen how changes in the topological character of the surfaces bounding a flow (e.g. an increase in connectivity) can create additional singular points in the flow pattern (as in flow around a building with a passageway underneath) or can produce a singularity in the shear-stress pattern where none existed before (as with the saddle-point singularity on the wall of a pipe where a junction with another is made).

To put this paper in perspective it should be remembered that topologically based kinematical theorems do not lead to solutions to the dynamical problems of fluid mechanics. But they may help us to use experimental and computational information more effectively to that end. In that sense these theorems may have a similar role to that of catastrophe theory!

We are grateful for financial support from the Building Research Establishment (to C.J.A.), the National Science Foundation (to J.C.R.H. and J.A.P.) and the N.A.S.A. Marshall Space Flight Center (to J.A.P. and H.W). We are also grateful for helpful suggestions from Professor M. Van Dyke, Mr A. J. Casson, Professor J. E. Cermak and from the referees.

REFERENCES

BATCHELOR, G. K. 1967 *An Introduction to Fluid Dynamics*. Cambridge University Press.

CASTRO, I. & ROBINS, A. 1977 The flow around a surface-mounted cube in uniform and turbulent streams. *J. Fluid Mech.* **79**, 307.

CODDINGTON, E. A. & LEVINSON, N. 1955 *Theory of Ordinary Differential Equations*. McGraw-Hill.

COUNIHAN, J., HUNT, J. C. R. & JACKSON, P. S. 1974 Wakes behind two-dimensional surface obstacles in turbulent boundary layers. *J. Fluid Mech.* **64**, 529.

FLEGG, G. C. 1974 *From Geometry to Topology*. English Universities Press.

FURUYA, Y. & MIYATA, M. 1972 Visual studies on the wake of a roughness element proximate to a wall. *Mem. Fac. Engng, Nagoya Univ.* **24**, 278.

GAUDET, L. & WINTER, K. G. 1973 Measurements of the drag of some characteristic aircraft excrescences immersed in turbulent boundary layers. *R.A.E. Tech. Mem. Aero.* no. 1538.

GREGORY, N. & WALKER, W. S. 1955 The effect on transition of isolated excrescences in the boundary layer. *Aero. Res. Counc. R. & M.* no. 2779.

HALITSKY, J. 1968 Gas diffusion near buildings. In *Meteorology and Atomic Energy*, p. 221. U.S.A.E.C.

LEGENDRE, R. 1965 Streamlines in a continuous flow. *Recherche Aérospatiale* no. 105, p. 3.

LIGHTHILL, M. J. 1963 In *Laminar Boundary Layers* (ed. L. Rosenhead), pp. 48–88. Oxford University Press.

MALTBY, R. L. & KEATING, R. F. A. 1962 The surface oil flow technique for use in low speed wind tunnels. *AGARDOGRAPH* no. 70.

MAULL, D. J. & EAST, L. F. 1963 Three-dimensional flow in cavities. *J. Fluid Mech.* **16**, 620.

MOCHIZUKI, M. 1961 Smoke observations on boundary layer transition caused by a spherical roughness element. *J. Phys. Soc. Japan* **16**, 995.

MOFFATT, H. K. 1964 Viscous and resistive eddies near a sharp corner. *J. Fluid Mech.* **18**, 1.

MONIN, A. S. & YAGLOM, A. M. 1971 *Statistical Fluid Mechanics*, vol. 1. M.I.T. Press.

NORMAN, R. S. 1975 Visualisation of local flow fields using scale models. *Proc. 2nd U.S. Nat. Conf. Wind Engng Res., Fort Collins*, pp. IV–3–1.

PERRY, A. E. & FAIRLIE, B. D. 1974 Critical points in flow pattern. *Adv. Geophys.* B **18**, 299.

SHARAN, V. KR. 1975 On characteristics of flow around building models with the view of simulating the minimum fraction of the boundary layer. *Int. J. Mech. Sci.*

SMITH, J. H. B. 1972 Remarks on the structure of conical flow. *Prog. Aero. Sci.* **13**, 241.

SMITH, J. H. B. 1975 A review of separation in steady, three-dimensional flow. *AGARD Conf. Proc.* no. 168, paper 31.

SQUIRE, L. C. 1962 The motion of a thin oil sheet under the boundary layer on a body. *AGARDOgraph* no. 70.

THWAITES, B. (ed.) 1960 *Incompressible Aerodynamics*. Oxford University Press.

WERLÉ, H. 1975 Ecoulement décollés: étude phénomenologique à partir de visualisations hydrodynamiques. *AGARD Conf. Proc.* no. 168, paper 38.

WOO, H. G. C., PETERKA, J. & CERMAK, J. E. 1976 Wind tunnel measurements in wakes of structures. *Colorado State Univ. Rep.* CER75-76HGCW-JAP-JEC40.

YU, C. C. T. 1975 Flow round a square block: measurement of mean and fluctuating pressure; effect of incident turbulence. M.Sc. dissertation, Dept. of Aeronautics, Imperial College.